IEEE Access
Multidisciplinary | Rapid Review | Open Access Journal

Received 3 January 2024, accepted 12 January 2024, date of publication 19 January 2024, date of current version 29 January 2024.

Digital Object Identifier 10.1109/ACCESS.2024.3355955

RESEARCH ARTICLE

WAVES: Soft-Material Based Adaptable Walking-Type Stair-Climbing Robot for Various Step Sizes

SUNGJUN PARK, JEONGPIL SHIN, (Member, IEEE), YOUNGHWAN KIM, AND TAEWON SEO, (Senior Member, IEEE)

School of Mechanical Convergence Engineering, Hanyang University, Seoul 04763, Republic of Korea

Corresponding author: Taewon Seo (taewonseo@hanyang.ac.kr)

This work was supported by the National Research Foundation of Korea (NRF) funded by the Ministry of Science and ICT for Bridge Convergence Research and Development Program under Grant NRF-2021M3C1C3096807 and Grant NRF-2021M3C1C3096808.

ABSTRACT Existing state-of-the-art stair climbing robots require precise control through many sensors and actuators to climb various stairs. In this study, we propose WAVES, a stair-climbing robot that can climb a variety of stairs with minimal electronic components and control. WAVES' stair climbing ability is due to its soft part on the bottom, which adapts passively to the shape of the stairs. The soft parts were fabricated into a compliant mesh shape and could be freely deformed according to the shape of the stairs. We used the ratio of horizontal and vertical reaction forces that occur when the soft part is deformed as an index to determine stability, and the simulation results showed that the arc shape has the smallest horizontal reaction force ratio of 0.224 (honeycomb: 0.303, spoke: 0.276). Also, to determine the appropriate strength of the soft parts, we calculated the maximum compressive force that each section of the soft part should withstand. Based on the calculation results, we made the gap between arc patterns closer where the strong compressive force is applied. In conclusion, before applying soft parts to the robot, the diagonal length of the stairs it could climb was 328.7 mm–350 mm, but after applying soft materials, it can climb all stairs under 400 mm.

INDEX TERMS Stair climbing, mobile robots, soft robotics, compliant mechanisms, four-bar linkage, service robots.

I. INTRODUCTION

For robots, climbing stairs is a long-standing problem. To replace or assist people, robots should be able to move in environments where people pass by, including stairs. Most robots use wheels for efficient movement; however, it is difficult for them to climb stairs. The reconfigurable mobile robot [1] overcomes obstacles by changing the width and length of the robot. When the reconfigurable mobile robot encounters a narrow step, it can increase the width of the body to overcome the obstacle without having to climb it. The inverted pendulum robot with planetary wheel mechanism [2] and Ascento Pro [3] are wheeled robots that can climb stairs by moving their center of gravity. However, in order for these robots to climb stairs, the radius of the wheels must be much higher than the riser of the stairs. Instead of large wheels, wheel clusters can be used. The motorized wheelchair [4] and the MSRox [5] climb stairs using a wheel cluster made of three wheels combined. Power is transmitted to each wheel through gears, and when the wheel reaches a step, the wheel cluster rotates and another wheel touches the next step. In this method, slippage occurs depending on the size of the stairs. Shino et al. solved the slippage problem by creating an inverted pendulum type robotic wheelchair that uses only a pair of wheel clusters consisting of two wheels [6]. However, the small contact surface reduces the stability of the robot and requires high friction on the stairs. Using additional actuators to lift the body upward allows the robot to climb stairs even with small, ordinary wheels. Scissor stair climbing robot [7] lifts the robot's body through a fork lift scissors mechanism and pushing the body to the next step. Also, Liu et al. designed a step-climbing robot that can quickly climbs stairs by folding the wheels and lifting the body with air cylinder pistons [8]. Such robots must stand on a single stair, so thier size is limited and they cannot climb small stairs. Therefore, Ma et al. proposed a stair-climbing robot [9] that can climb small stairs by lifting the robot body and adjusting the height of the wheels through six linear actuators.

The associate editor coordinating the review of this manuscript and approving it for publication was Agustin Leobardo Herrera-May.

However, this type of robot requires too many actuators and takes a long time to climb high stairs. There have been many attempts to use the wheel to climb stairs, but the wheels are less stable on steps and highly dependent on the friction force.

Instead of wheels, tracks have been widely used for overcoming rough terrain and climbing stairs. The track climbs the stairs by anchoring the outer grousers to the stair edges. Wheel-track hybrid EPW [10] and Scewo BRO [11] are wheelchairs that climb stairs using tracks. However, since tracked robots can only climb stairs when the grousers can reach the edge on the first step, to climb high stairs, the track needs to be huge, or a separate actuation to lift the track is needed. The tracked robot designed by Dong et al. climbs stairs by attaching a swing arm so that the grouser can reach stairs larger than the track [12]. Liu et al. presented RLMA [13], which can climb high stairs by changing the shape of the track using flippers inside the track. Tracked robots are a suitable stair climbing method when carrying heavy payloads such as wheelchairs due to their sturdy structure and energy efficiency. However, because the grouser shape of the track is fixed, several problems arise. The spacing of the grousers is different from the spacing of any stairs; therefore, slip occurs, and the track can only grip one stair [14]. This problem reduces stability and damages the edges of the stairs.

Legged robots recently attracted attention due to their high mobility performances under various operational conditions. Legged robots, i.e., HyTRo-I [15], ANYmal [16], and Spot [17], demonstrate a high capacity to overcome obstacles via gait control. However, legged robots require many actuators corresponding to the high degree of freedom. In addition, for legged robots to climb stairs, exact information is required, such as the stairs size and location of the robot and the stairs. Therefore, various sensors (RAdio Detection And Ranging, Light Detection and Ranging, etc.) are essential and complex control systems are required.

Existing stair-climbing mechanisms exhibit low adaptability to various environments or have extremely complex systems. Several studies were recently conducted using soft materials with high adaptability and low complexity. Given that a flexible body operates passively, it exhibits high shape adaptability with fewer actuators and simple control techniques. In particular, soft grippers demonstrated a high adaptability based on compliant materials and mechanisms [18], [19], [20], [21]. Rigid grippers require accurate information regarding the shape and location of things, in addition to the strategies for holding things. Therefore, many sensors and complex controls are essential. In contrast, soft grippers require simpler information on the location of the object. Just as grippers achieved high adaptability and low complexity through soft materials, there have been attempts to apply soft materials to step-overcoming mechanisms.

NAMU [22] from Hyundai Motor Company, is a personal mobility device for climbing stairs with soft airless tires. Airless tires maximize the ability to overcome stairs by allowing the wheels to freely deform to match the shape of the stairs. High-grip crawlers [14] and the Amoeba GO-1 [23] are robots with soft materials, which are applied to track-based robots. The soft materials attached to the tracks deform according to the shape of the steps. Therefore, the tracks can grip multiple steps evenly and no slip occurs.

We applied soft material to WAVE [24], which is a stair-climbing robot based on four-bar linkages, as shown in Fig. 1. The four-bar linkage structure has the ability to overcome obstacles with a simple structure [25], [26]. Four-bar linkage is also possible to implement continuous walking motion [27], [28]. At the bottom of WAVE, grooves were made to fit the shape of the stairs, such that they stably settled on the edge of the stairs. When the front and rear cranks rotate, the body and legs rotate parallel to each other and alternatively step up stairs. WAVE provides the advantage of a simple structure and requires a small coefficient of friction. However, because the grooves are fixed, WAVE can only climb stairs with limited dimensions. To overcome this limitation, we developed WAVES with soft feet, as shown in Fig. 2.

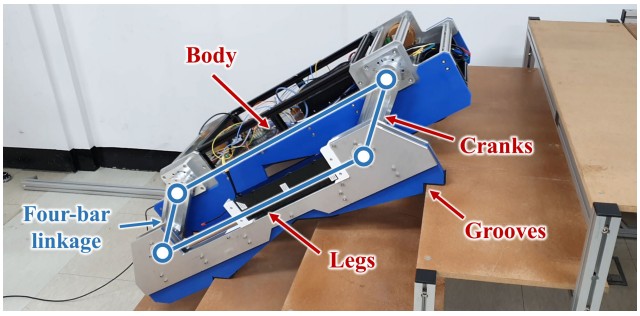

FIGURE 1. Configuration of the four-bar linkage robot WAVE.

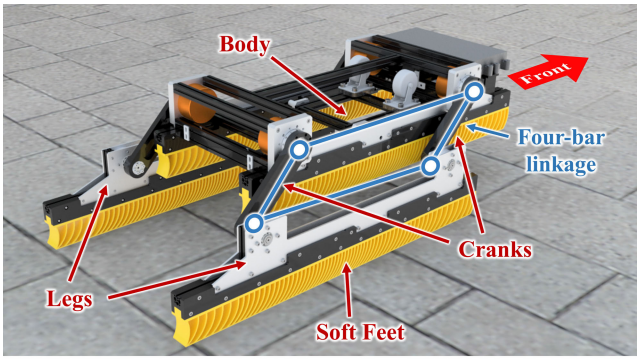

FIGURE 2. Soft material-based robot, WAVES.

The soft feet were made of compliant meshes. Unlike other traditional stair climbing robots, WAVES doesn't require a detailed analysis of the environment and precise controls. Given that soft feet deform passively, WAVES can easily adapt to a variety of stairs. In addition, due to the soft material, climbing stairs is quiet, stable, and does not damage the stairs. However, by simply applying soft materials such as sponges, a robot cannot climb stairs. An appropriate shape

and strength of the soft parts are required for the robot. When a soft material is deformed, the reaction forces act accordingly. The reaction forces push the robot away from the stairs, thus causing it to fall. Additionally, breakage occurs if the soft material is not sufficiently strong to withstand the robot's action. This paper presents the process of determining the shape of soft feet. We performed a finite element analysis based on an Ansys simulation to determine the appropriate shape of the soft feet. In addition, the required strength of the soft feet was calculated by considering four variables that determine the force to be withstood by the soft feet. Given that the force applied to each position of the soft feet was different, we developed an appropriate shape by adjusting the density of the compliant mesh accordingly.

Section II details the structure and operation of WAVE, a related study. The structure and climbing mechanism of WAVES are described in Section III. Section IV describes the soft foot design process. The prototype fabrication and experimentation are introduced in Section V. Finally, Section VI presents a summary of the study and discussion of future work.

II. RELATED WORK

In this section, we review previous studies. The robot most closely related to our research is WAVE. WAVE has a four-bar linkage structure for stair climbing ability. As shown in Fig. 1, the body and leg of WAVE, and the two cranks connecting them, form a parallelogram four-bar linkage structure. In addition, the bottom part of the WAVE there are grooves made to match the shape of stairs, so the robot can stand stably on the tread of the stairs. If all cranks rotate in the same phase, the body and legs rotate parallel to each other. When the body is touching the stairs, the legs rotate to move to the next step, and when the legs touch the step, this time the body rotates to reach the next step. As a result, the robot's body and legs alternately touch the stairs and climb the stairs, just as people contact their feet alternatively to the step when climbing stairs. Stair climbing method through a four-bar linkage structure of WAVE has many advantages in simplicity and stability.

Table 1 shows a comparison of specifications of related studies mentioned in Section I. Where h, w, ϕ are the height, width, and slope of the stairs, respectively, and $R = \sqrt{h^2 + w^2}$. The ''complexity of the mechanism'' is the number of joints multiplied by the number of actuators [29], [30]. The ''required information'' and ''control complexity'' are the minimum level of information and control required to automate stair climbing. In wheeled robots, the inverted pendulum shape allows the robot to climb stairs by moving the center of gravity of the robot forward of the wheels [2], [3], [6]. Inverted pendulum robots have relatively low mechanical complexity but high control complexity. Four pairs of wheel clusters can be used to climb stairs with much lower control complexity [4], [5]. However, wheel clusters have many joints, making the mechanism much more complex. Similarly, using separate actuators to lift the body has a low control complexity but a high mechanism complexity [7], [8], [9]. Tracked robots can climb stairs with low complexity of mechanism and simple controls [12], [13]. However, if they are carrying heavy loads, they will need additional actuation to assist them in entering and exiting the stairs, increasing the complexity of mechanism [10], [11], [14]. Legged robots can climb almost any stairs due to their high degree of freedom [15], [16], [17]. The trade-off is high complexity of mechanism and high control complexity.

WAVE can climb stairs with relatively low mechanical and control complexity. Compared to the wheeled robots, WAVE is stable as it requires a much smaller coefficient of friction, 0 in a stationary state and about 0.2 when climbing stairs. Also, unlike tracked robots, WAVE guarantees that it always touches two stairs when climbing stairs. While tracked robots concentrate the load on one edge of the stairs, WAVE does not damage the stairs because it stands on the treads. Additionally, compared to legged robots, WAVE implements walking-like motion with a much simpler structure and control method. However, WAVE's grooves have a fixed shape, so there is a problem that robots cannot climb stairs of various sizes due to their low adaptability. To solve the problem of low adaptability, we propose WAVES with soft feet in this study. WAVES has high adaptability because its soft feet adapt to stairs of various sizes. Also, while many modern stair-climbing robots require many sensors to know the exact shape and location of the stairs and precise control of many motors, WAVES can passively adapt and climb stairs just by rotating four cranks simultaneously without a complicated control method.

The detailed comparison of stair climbing performance is described in Section V.

III. STRUCTURE AND STAIR-CLIMBING MECHANISM OF WAVES

This section introduces the structure of WAVES. And WAVES' stair-climbing method is divided into three steps and explained in detail.

A. ROBOT STRUCTURE

Fig. 2 presents the structure of WAVES. WAVES has the same four-bar linkage structure as WAVE. WAVES has two legs with an interjoining body. Moreover, it has four cranks that rotate its body and legs. The lower part of the robot has 'soft feet' that freely deform according to the shape of the stairs. Furthermore, WAVES has two in-wheel motors and two castor wheels for flatland movement, which are designed to be stored inside the robot to prevent contact with the stairs while climbing them. Given that soft feet are deformed by the edges of stairs, the distance between the edges of the stairs is critical. The objective was to climb stairs with a diagonal length of up to 400 mm, as the distance between typical stair edges is about 320–360 mm. The length of the soft feet was set to 850 mm because the length of the soft feet should exceed 800 mm, to ensure stepping on a minimum of two steps. Soft, strong polyurethane (PU) was used to support the mass of the WAVES system, which was approximately 30 kg.

TABLE 1. Comparison with related works.

Type	Name	Complexity of mechanism	Time to climb a step (sec)	Climbable stairs (mm)	Required information	Control complexity
Wheeled robot	Planetary wheel mechanism [2]	8	2.4	$h \leq 200$	None	Medium (Inverted pendulum)
	Motorized wheelchair [4]	115	-	$h \leq 210$	Position of the first and last step	Medium-low
	MSRox [5]	196	1.33	$h \leq 170$	None	Low
	Robotic wheelchair [6]	36	3	$h \leq 225$, $w \geq 260$	Position of each riser	Medium-high (Inverted pendulum)
	Step-climbing robot [8]	96	1-2	$h \leq 200$, $w \geq 1200$ (w: estimated)		Low
	Scissor stair climbing robot [7]	128	-	$h \leq 200$, $w \geq 700$ (w: estimated)	Position and height of each riser	Medium-low
	Stair-climbing robot [9]	140	-	-		
Tracked robot	Wheel-track hybrid EPW [10]	384	0.7	$h \leq 170$, $R \leq 350$ (R: estimated)	Position of the first and last step	
	Scewo BRO [11]	64	2	$h \leq 200$ $20° \leq \phi \leq 36°$		
	Tracked robot [12]	16	-	$R \leq 430$ (estimated)		
	RLMA [13]	18	13.5	$h \leq 200$, $R \leq 515$ (h, R: estimated)		
	High-grip Stair Climber [14]	48	0.7	$h \leq 200$, $R \leq 310$ (h, R: estimated)	Position of the last step	
Wheel-legged robot	Ascento Pro [3]	40	1	Almost any stairs	Position and height of each step	High (Inverted pendulum)
Legged robot	HyTRo-I [15]	224	-		Width, height, and position of each step	High
	ANYmal [16]	144	1			
	Spot [17]	144	1			
Four-bar linkage robot	WAVE [24]	32	2	$328.7 \leq R \leq 350$	Position of the first step	Low
	WAVES	32	2	$R \leq 400$		

B. STAIR-CLIMBING MECHANISM

WAVES stair-climbing involves three steps: entering, climbing, and exiting.

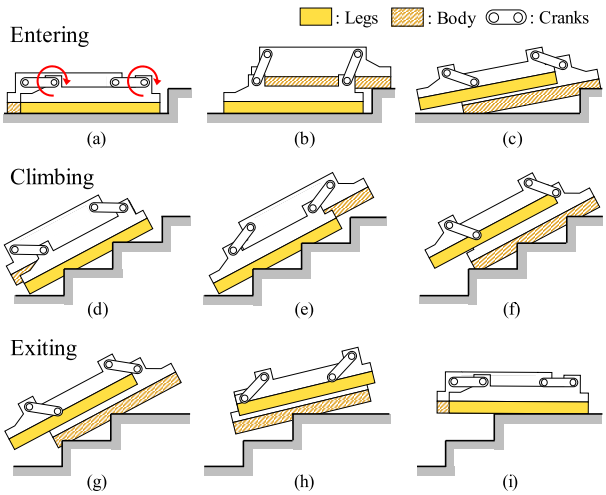

FIGURE 3. The process of WAVES climbing the stairs.

1) ENTERING

Fig. 3 (a)–(c) presents the case of entering the stairs. When WAVES reaches the front of the stairs, the cranks start rotating in the same direction and phase. Then, as shown in Fig. 3 (b), the front part of the body is in contact with the nosing of the first step. As the crank rotates further, the legs rise, as shown in Fig. 3 (c), and the entire robot tilts toward the stairs. When the cranks rotate twice, the angle of the WAVES is equal to the slope of the stairs, and the WAVES settles on the stairs, as shown in Fig. 3 (d).

2) CLIMBING

Fig. 3 (d)–(f) presents the process of climbing. As shown in Fig. 3 (d)–(e), when the legs are stepping on the stairs, the body moves forward as cranks rotate. In Fig. 3 (f), the body touches the stairs, and in this case, the legs move along the cranks. When the cranks rotate by half a turn, the body and legs alternately step up the stairs.

3) EXITING

Fig. 3 (g)–(i) presents WAVES exiting the stairs. The location of the center of gravity of WAVES changes according to the

rotation angle of the cranks. As shown in Fig. 3 (g)–(h), as the legs (or body) move forward, the center of gravity of WAVES moves forward. As a result, WAVES gradually tilts parallel to the floor and exits the stairs.

IV. SOFT FEET DESIGN

In this section, we describe the entire process of designing soft feet. We discuss the performance index of the soft feet and the role they play in climbing stairs. In addition, to fabricate soft feet with appropriate strength, it is necessary to know the amount of reaction force that soft feet must generate while climbing stairs. In this subsection we also define the variables that determine the reaction force and calculate the magnitude of the forces applied at each location of the soft feet.

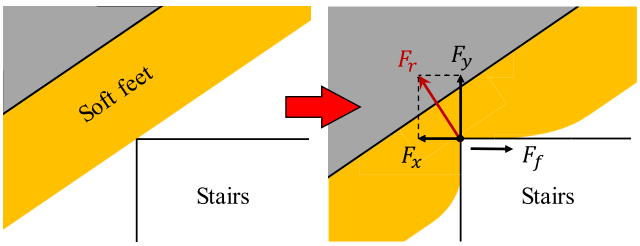

FIGURE 4. Free-body diagram of compressed soft feet. A description of the symbol is provided in the text.

A. PATTERN DECISION

When the soft feet touch the edge of the stairs and are deformed, a reaction force is generated due to the deformation. If the soft feet are made of a simple sponge-like material, the reaction force F_r acts in the direction opposite to the pressed direction, as shown in Fig. 4. Moreover, F_y supports the robot's weight and F_x pushes it off the stairs. If the frictional force F_f is in equilibrium with F_x, the robot settles on the stairs. However, if F_x exceeds the maximum F_f, the soft feet cannot grip the stairs. Therefore, when pressed by stairs, F_x should be maximally small, such that the soft feet can stably grip the stairs.

To control the physical properties, we made soft feet into a compliant mesh form. Compliant meshes are widely used in airless tires. The most widely used airless tire patterns are arc [31], [32], honeycomb [33], and spoke [34] shapes. And these three patterns are the simplest forms that include other forms. As shown in Fig. 5, we made three patterns of soft feet samples. Fig. 5 (a) is an arc-shaped sample that represents a curved pattern and exerts a large vertical force relative to the horizontal force when deformed. The arc shape can readily predict the extent and direction of deformation. The honeycomb pattern shown in Fig. 5 (b) represents closed curves that resemble circles. The honeycomb pattern can form a solid structure with slight material, and demonstrate excellent fatigue resistance [35]. The last pattern shown in Fig. 5 (c) is a simple spoken form and it represents patterns in triangles or other straight lines. All three samples were prepared with a thickness of 2 mm and an interval of 13 mm. Thereafter, by pressing the three samples, the horizontal and vertical reaction forces were measured via an Ansys simulation. The measurement results and ratios of the horizontal and vertical reaction forces are listed in Table 2. The reaction force ratio corresponds to the coefficient of friction required for each pattern to avoid slipping on the stairs.

TABLE 2. Ansys simulation results of reaction forces for three patterns.

	Arc	Honeycomb	Spoke
Volume (cm^3)	15.4	20.7	26.6
x-direction: Horizontal force (N)	0.487	8.92	1.99
y-direction: Vertical force (N)	2.17	29.4	7.21
Reaction forces ratio (x/y)	0.224	0.303	0.276
(Vertical force)/(Volume) (N/cm^3)	0.141	1.42	0.271

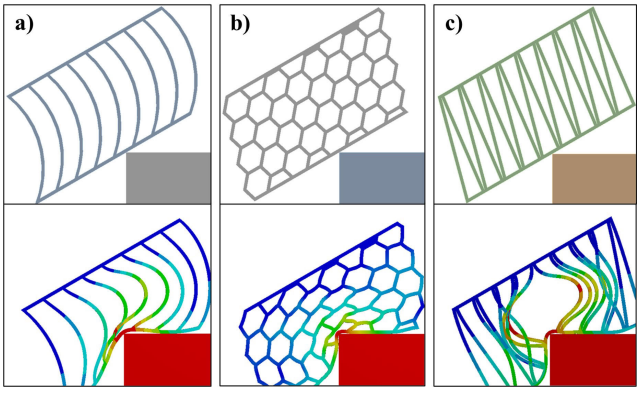

FIGURE 5. Ansys simulation. (a) Arc, (b) honeycomb, (c) spoke pattern.

As expected, the honeycomb pattern can support significantly large vertical forces relative to the amount of material used. Therefore, the honeycomb pattern is the most appropriate when heavy weights are to be supported. However, the reaction force ratio in the x-direction was the smallest for the arc pattern. In addition, given that the angle, thickness, and shape of the arc pattern can be readily adjusted, we developed soft feet using an arc pattern.

B. FOUR AREAS OF SOFT FEET

If the strength of the soft feet is insufficient, they are damaged by the weight of WAVES. However, if the soft feet are excessively hard, they may not deform appropriately when touching the stairs. We considered the role of each part of the soft feet and the magnitude of the force that the soft feet with need to support. Fig. 6 presents the overall appearance of the soft feet. Soft feet comprise four areas: two-point contact, front, middle, and rear.

1) TWO POINTS CONTACT AREAS

When WAVES climbs the stairs, the number of points in contact with the stairs is typically two or three. It is clear that soft feet support greater forces when they contact at two points than at three points. Therefore, the two points contact areas, which are the areas in contact with the stairs at the two points, are required to support a larger force than the other

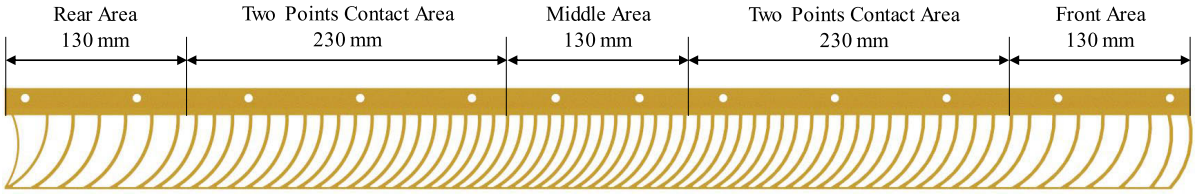

FIGURE 6. Overall appearance of soft feet with four areas.

areas during climbing. We calculated the maximum force that the two-point contact area should support, and the process and results are presented in the next subsection.

2) FRONT AREA AND REAR AREA

While climbing, the front and rear areas contact the stairs only when the soft feet touch the stairs at the three points. Therefore, they are subject to smaller forces than those in the two-point contact area. However, as shown in Fig. 3 (c), in entering, the front and rear areas should support the overall weight of the robot. The maximum force applied to the front and rear areas is described in the next subsection.

3) MIDDLE AREA

The middle area plays an important role in exiting. During the exit, as shown in Fig. 3 (h), only the middle area touches the stairs to support the robot's weight. Therefore, in the middle area, the spacing of the mesh was made sufficiently dense to withstand the weight due to the WAVES.

C. REACTION FORCES

In order to fabricate soft feet with appropriate strength, it is necessary to know the amount of reaction force that soft feet must generate while climbing stairs. In this subsection, we define the variables that determine the reaction force and calculate the magnitude of the forces applied at each location of the soft feet.

1) VARIABLES

The magnitude of the force that the WAVES is required to support while climbing stairs is determined by the shape of the stairs and the position of the center of gravity.

The height h of the most commonly seen stairs is 160–180 mm, and the width w is 280-310 mm. Thus, the minimum value of the diagonal length of the stairs was $\sqrt{160^2+280^2} = 322.49$, and the maximum value was $\sqrt{180^2+310^2} = 358.47$. Therefore, we set the range of variables as shown in Table 3.

Due to the four-bar linkage structure of WAVES, the position of the center of gravity changes with the rotation angle of the cranks. Fig. 7 (a) presents the position of the center of gravity of the body, legs, and cranks. It should be noted that **B** and **L** are the centers of gravity of the body and legs, respectively; $\mathbf{C_1}$ and $\mathbf{C_2}$ are the centers of gravity of the cranks; and b_x, b_y, and l_x, l_y indicate the positions of the center of gravity of the body and crank legs relative to the joint, respectively. Furthermore, c is the length of the crank and the center of gravity of the crank at its center, and the

TABLE 3. Specification of variables.

Parameter	Range	Units
Stair diagonal length, R	$320 \le R \le 360$	mm
Stair height, h	$160 \le h \le 180$	mm
Rotation angle of cranks, θ	$0 \le \theta < 180$	deg
Position pressed by stairs, s	$850 - 2R \le s \le R$	mm

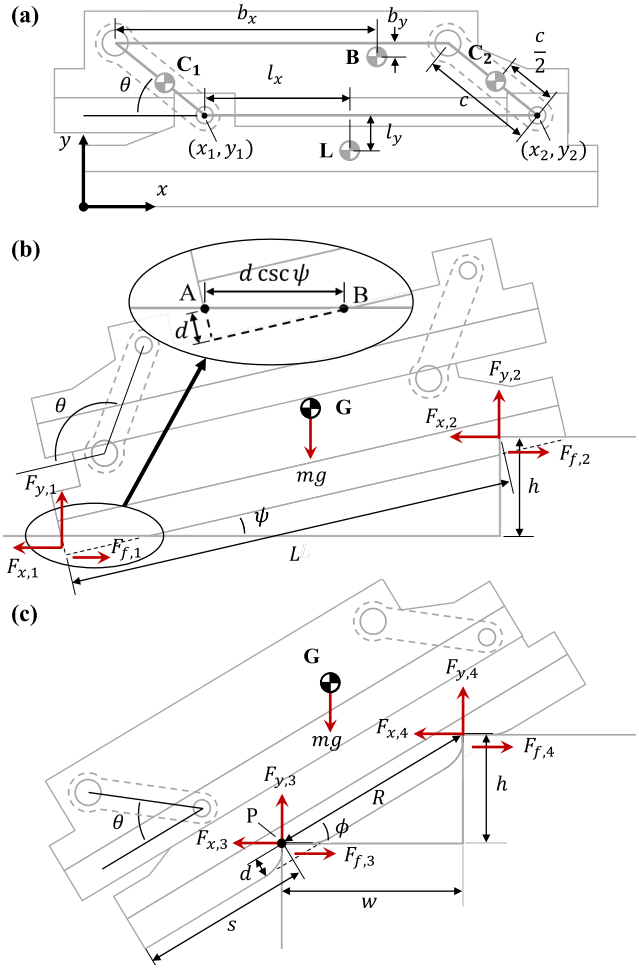

FIGURE 7. (a) The center of gravity of the body(B), crank legs(L), and cranks(C_1, C_2). In addition, (x_1, y_1) and (x_2, y_2) are the positions of the joints, and θ is the rotation angle of the cranks. Free-body diagrams of WAVES in (b) Entering and (c) Climbing. Descriptions of symbols are in the main text.

coordinates of each center of gravity were obtained using θ and the rotation angle of the crank.

$$\mathbf{B} = \begin{bmatrix} x_1 + b_x - c\cos\theta \\ y_1 - b_y + c\sin\theta \end{bmatrix} \tag{1}$$

$$\mathbf{L} = \begin{bmatrix} x_1 + l_x \\ y_1 - l_y \end{bmatrix} \tag{2}$$

$$\mathbf{C_1} = \begin{bmatrix} x_1 - \frac{c}{2}\cos\theta \\ y_1 + \frac{c}{2}\sin\theta \end{bmatrix} \tag{3}$$

$$\mathbf{C_2} = \begin{bmatrix} x_2 - \frac{c}{2}\cos\theta \\ y_2 + \frac{c}{2}\sin\theta \end{bmatrix} \tag{4}$$

Consequently, the total center of gravity $\mathbf{G}$ of the WAVES is expressed as follows:

$$\mathbf{G} = \begin{bmatrix} x_G \\ y_G \end{bmatrix} = \frac{1}{m}\left(m_b\mathbf{B} + m_l\mathbf{L} + m_c\left(\mathbf{C_1} + \mathbf{C_2}\right)\right) \tag{5}$$

In (5), m_b, m_l, and m_c represent the weight of the body, the pair of crank legs, and the pair of cranks, respectively; and m represents the total WAVE weight because there are two pairs of cranks, $m = m_b + m_l + 2m_c$.

2) REACTION FORCES ON FRONT AREA AND REAR AREA

When the lower part of the robot is made of rigid material, there are only two forces acting in a stationary state: gravity and the reaction force of the stairs supporting the robot [24]. However, in the case of WAVES, by the movement of the crank, the soft feet are compressed in a diagonal direction and a reaction force against the compression acts. During that time, compression proceeds until the y-direction component of the reaction force is in equilibrium with gravity. Compression stops when the y-direction reaction force is sufficient to support the robot's weight. Additionally, frictional force acts to offset the x-direction reaction force. As shown in Fig. 7 (b), soft feet are subject to reaction forces $F_{x,i}$, $F_{y,i}$ (i=1, 2) from the stair edge and floor during entering. But the position at which the reaction forces act and the degree of compression of the soft feet can be obtained only when the design of the soft feet is determined. Therefore, we introduced the following assumptions to calculate $F_{x,i}$ and $F_{y,i}$:

1) Forces act on the edges of the stairs or at the position that maximizes the reaction force.
2) The compression distance of soft feet is $d = 30$ mm.
3) x-directional reaction forces due to the deformation of the soft feet are in equilibrium with the frictional forces.

It should be noted that $F_{y,2}$ has a maximum value $F_{y,2,max}$ when $F_{y,1}$ is applied to Point A in Fig. 7 (b). The formula for calculating $F_{y,2,max}$ is

$$\begin{aligned} \sum M_A &= F_{y,2,max}\,L\cos\psi + \left(F_{x,2} - F_{f,2}\right)h \\ &\quad - mg\left(x_G\cos\psi - y_G\sin\psi\right) = 0 \\ F_{y,2,max} &= \frac{mg\left(x_G\cos\psi - y_G\sin\psi\right)}{L\cos\psi} \end{aligned} \tag{6}$$

where L denotes the distance from the heel of the leg to the edge of the stairs, ψ denotes the slope of the robot, and $\tan\psi = h/L$.

Moreover, $F_{y,1}$ has a maximum value $F_{y,1,max}$ when $F_{y,1}$ is applied to Point B. Given that $F_{y,1} + F_{y,2} = mg$, the equation for obtaining $F_{y,1,max}$ is expressed as follows:

$$F_{y,1,max} = \frac{mg\left(L\cos\psi - x_G\cos\psi + y_G\sin\psi\right)}{L\cos\psi - d\csc\psi} \tag{7}$$

Fig. 8 is a graph displaying $F_{y,1,max}$, $F_{y,2,max}$ according to the height of the stairs h.

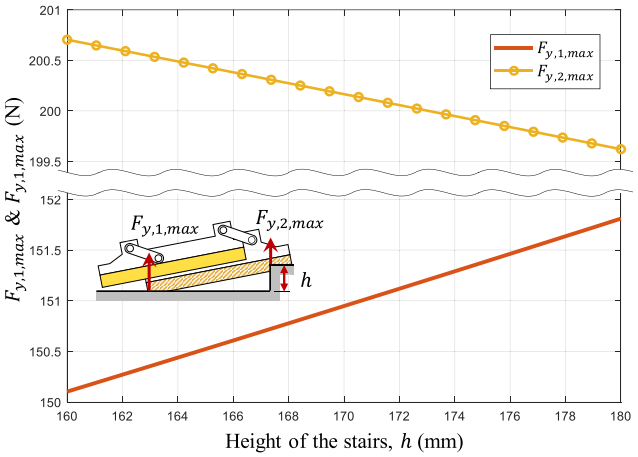

FIGURE 8. Maximum y-direction reaction forces according to the stair height.

3) REACTION FORCES ON TWO POINTS CONTACT AREAS

As shown in Fig. 7 (c), the soft feet are subject to reaction forces $F_{x,j}$, $F_{y,j}$ (j = 3, 4) from the edge of the stairs during climbing. Point P is the point at which the soft feet and edges of the stairs meet, and $F_{y,j}$ can be obtained through the moment at Point P as follows:

$$\begin{aligned} \sum M_{\mathbf{P}} &= wF_{y,4} - mg\left((x_G - s)\cos\phi - (y_G - d)\sin\phi\right) \\ &\quad + h\left(F_{friction,4} - F_{x,4}\right) = 0 \end{aligned} \tag{8}$$

$$\begin{aligned} F_{y,4} &= \frac{mg}{w}\left((x_G - s)\cos\phi - (y_G - d)\sin\phi\right) \\ F_{y,3} &= mg - F_{y,4} \end{aligned} \tag{9}$$

where ϕ is the angle of inclination of the stairs and s is the distance between the heel of the legs and point P. Moreover, x_G and y_G are expressed as Eq. (5) about θ, and $w = \sqrt{R^2 - h^2}$. Therefore, $F_{y,i}$ is a function of the four variables $F_{y,j} = f_j(R, h, \theta, s)$ The ranges of each variable are shown in Table 3. Fig. 9 presents a graph of the maximum force applied to each position of the soft feet through Eq. (8) and (9). The black dotted lines in Fig. 9 represent the weight of the robot in mg. If the reaction force is equal to mg, only one point on the soft feet supports the entire weight of WAVES. In this case, the WAVES robot may tilt while the crank rotates. In particular, designing $F_{y,3} < mg$ is essential because of the risk of backward overturning when $F_{y,3} = mg$.

D. DETERMINING THE PARAMETERS OF SOFT FEET

Based on the calculation results in the previous subsection, we determined the soft feet parameters: Shape of arc pattern (thickness, radius, angle), and spacing of arc pattern.

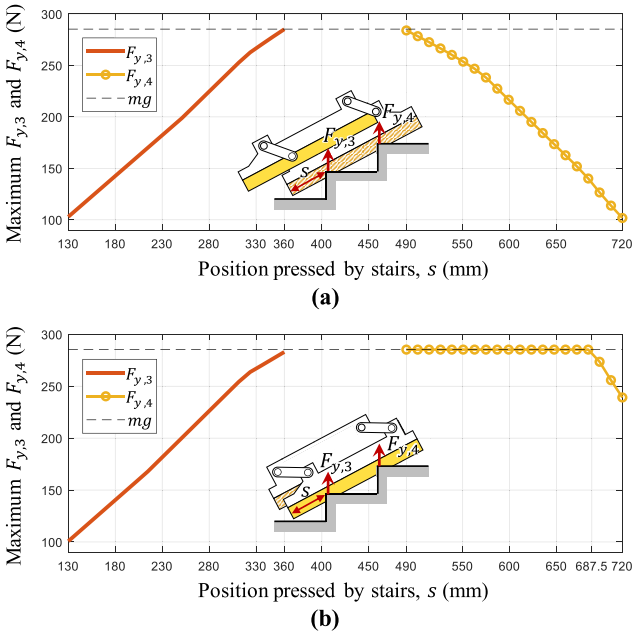

FIGURE 9. Maximum reaction forces, $F_{y,3}$ $F_{y,4}$, depending on pressed position, s. (a) When the legs of WAVES move. (b) When the body of WAVES moves.

1) SHAPE OF ARC PATTERN

Fig. 10 (c) shows the thickness, radius, and angle of the arc pattern. The larger the thickness and radius of the arc pattern, the greater the load that soft feet can withstand. However, if the arc is too thick, the distance between patterns must increase, so the deformation of soft feet becomes uneven. Also, to be able to fabricate it, the thickness of the arc must be over 2 mm, so we made soft feet with a thickness of 3 mm. In the case of radius, if the radius is large and the arc approaches a straight line, the soft feet may deform in the opposite direction from what we intended. Therefore, we determined the radius to be 55 mm so that it could withstand sufficient load and deform in the desired direction. Since the angles of the stairs shown in Table 3 range from 26.4°to 34.2°, we determined the arc angle to be 30°, which is close to the median. And this is also the average slope angle of common stairs.

2) SPACING OF ARC PATTERN

The material of the WAVES soft feet was made of PU. The used PU has a hardness of 85 Shore A and a tensile strength of 180 MPa. We built a test bench as shown in Fig. 10(a) to measure the reaction force produced by PU as it is compressed. The test bench consisted of a holder, a screw, a load cell, and a magnetic encoder. A holder secured both ends of the PU sample. The screw and magnetic encoder were connected to one side of the holder and the load cell was attached to the other side. When the screw was turned, the sample was compressed, and the load cell measured the reaction force. Simultaneously, the magnetic encoder measured the compressed distance. The PU sample had a width of 15 mm and the same arc shape as the soft feet,

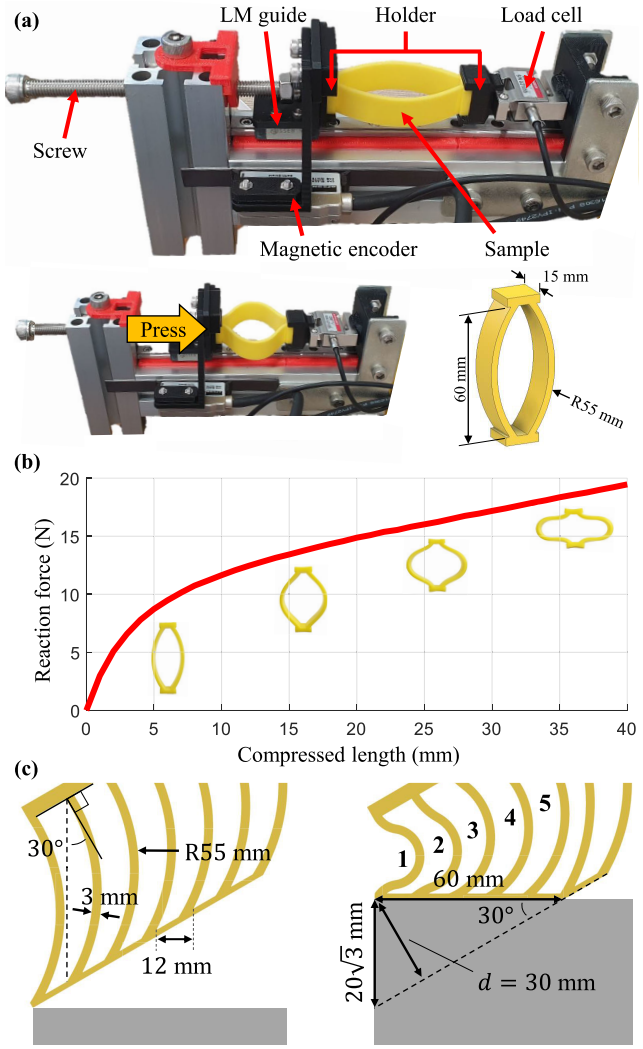

FIGURE 10. (a) Test bench to measure reaction force (b) Reaction force according to compressed length (c) Compressed soft feet.

with a thickness of 3 mm and a radius of 55 mm. Fig. 10 (b) is a graph displaying the magnitude of the reaction forces with respect to the compression distance. We determined the spacing of the soft feet pattern based on the compression test results. Fig. 10 (c) is a scematic showing an example of climbing stairs with a slope of 30°when the pattern spacing is 12 mm. The compression distances of the five arcs are $20\sqrt{3}$ mm, $16\sqrt{3}$ mm, $12\sqrt{3}$ mm, $8\sqrt{3}$ mm, and $4\sqrt{3}$ mm, respectively. We get the magnitude of the reaction force according to the compression distance through the graph of Fig. 10 (b), which is about 18.3 N, 16.7 N, 15.1 N, 13.1 N and 10.1 N, respectively and the total is 73.3 N. The compression test sample has two arcs with a width of 15 mm, and the WAVES have arcs with a width of 40 mm on both sides. Therefore, the reaction force generated by soft feet is $73.3 \times 40/15 = 195.5$ N. Fig. 11 is a graph showing the magnitude of the reaction force generated by soft feet according to the spacing between arc patterns. The graph bends where the intervals between arcs are 60/7 mm, 10 mm, 12 mm, and 15 mm, and these are when the number of arcs

TABLE 4. Hardware components specifications, part number (manufacturer).

Component	Specification, part number (manufacturer)
Crank motor (driver built-in)	BLDC motor, 36 V, 34 N·m, 30 rpm, GSA80-3650 (Motorbank)
In-wheel motor	24 V, 3 N·m, 300 rpm, MDH80 (MDrobot)
Controller	NI cRIO-9039 & NI 9862 (National Instruments)
Motor driver(wheel)	MD400T (MDrobot)
Convertor(24 V)	FIT0171 (DFROBOT)
Battery(36 V)	Li-ion battery, 18.2 Ah, Quick2 (INOKIM)
CAN Transceiver	SN65HVD230 (Waveshare)

to be compressed changes. We adjusted the spacing of the pattern according to the magnitude of the force each part of the soft foot receives. The magnitude of force received in the four areas of soft feet was calculated from the preceding subsection.

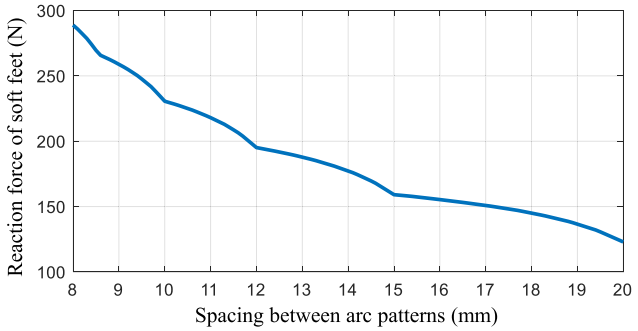

FIGURE 11. Graph showing the magnitude of the reaction force generated by soft feet according to the spacing between arc patterns.

V. ROBOT BUILDING AND EXPERIMENTATION

In this section, we organized the parts used in the robot construction and conducted experiments. Also, we compared the experimental results to the previous study.

A. PROTOTYPE FABRICATION

The WAVES prototype is illustrated in Fig. 12. The length of the crank to climb the first stair when entering is 190 mm, which is longer than that of the riser of common stairs. Parallelogram four-bar linkage structures that WAVES has enter singularity when all bars are aligned. To overcome this singularity, individual motors are connected to each crank. Under the WAVES, there are two in-wheel motors and two caster wheels for flat-ground driving, which can be stored inside when climbing stairs. Detailed hardware components are presented in Table 4. Fig. 12 (b) presents the external casing. Above the casing, the shelf can adjust its inclination up to 35°, according to the slope of the stairs.

We attached friction pads to the soft feet to prevent the robot from slipping on the stairs. The coefficient of friction between the friction pad and the stainless steel plate is 0.98 in a dry state and 0.84 in a wet state.

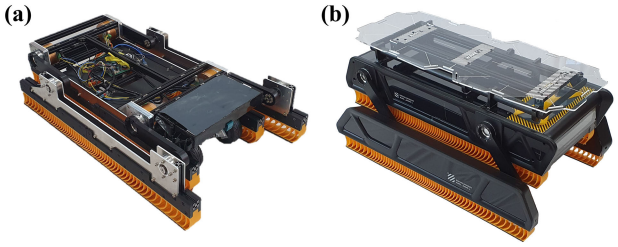

FIGURE 12. Frabricated (a) WAVES, and (b) WAVES with casing.

B. EXPERIMENTATION

We conducted stair-climbing experiments on seven different stairs. We confirmed performance improvement compared to previous studies by using the range of stairs that can be climbed as a performance matric.

1) ON THE TEST BENCH

We built a test bench as shown in Fig. 13 to evaluate the stair-climbing ability of WAVES. The test bench had a total of five steps to check all the entering, climbing, and exiting. The frame of the stairs had an aluminum profile with multiple holes to form stairs of various sizes. The sizes of the stairs that WAVES was set to climb were $280 \times 160\,\text{mm}^2$, $310 \times 160\,\text{mm}^2$, and $310 \times 180\,\text{mm}^2$. The rotational speed of the crank was 10 rpm, and it could climb all the stairs with six rotations. In the experiment, WAVES was able to climb all three stairs in 36 s. Among these, the $280 \times 160\,\text{mm}^2$ and $310 \times 180\,\text{mm}^2$ stairs are sizes that WAVE, which is a prior model without soft feet, cannot climb.

2) FIELD TEST

Fig. 14 shows field tests of WAVES on three outdoor stairs and one indoor stairs. Fig. 14 (e) shows how soft feet gradually deform while climbing stairs. Outdoor stairs are more dusty than indoor stairs, so there is a high risk of slipping. And even though the stairs in Fig. 14 (d) were concrete steps without anti-slip edges, WAVES climbed the stairs well without slipping. WAVES was successfully able to climb all four stairs.

3) COMPARISON WITH PREVIOUS STUDIES

The elements that determines the size of climbable stairs varies depending on the type of robot. For wheeled robots, the radius of the wheels, or cluster of wheels, determines the size of the stairs the robot can climb [2], [3], [4], [5], [6]. Larger wheels and wheel clusters increase the height of the stairs the robot can climb, but the torque required from the motor increases proportionally. If the wheels are small, a separate actuator can be used to lift the body to climb the stairs. Smaller wheels can also be used to climb tall stairs with separate actuators [7], [8], [9]. However, these methods usually require the entire robot body to be on a single

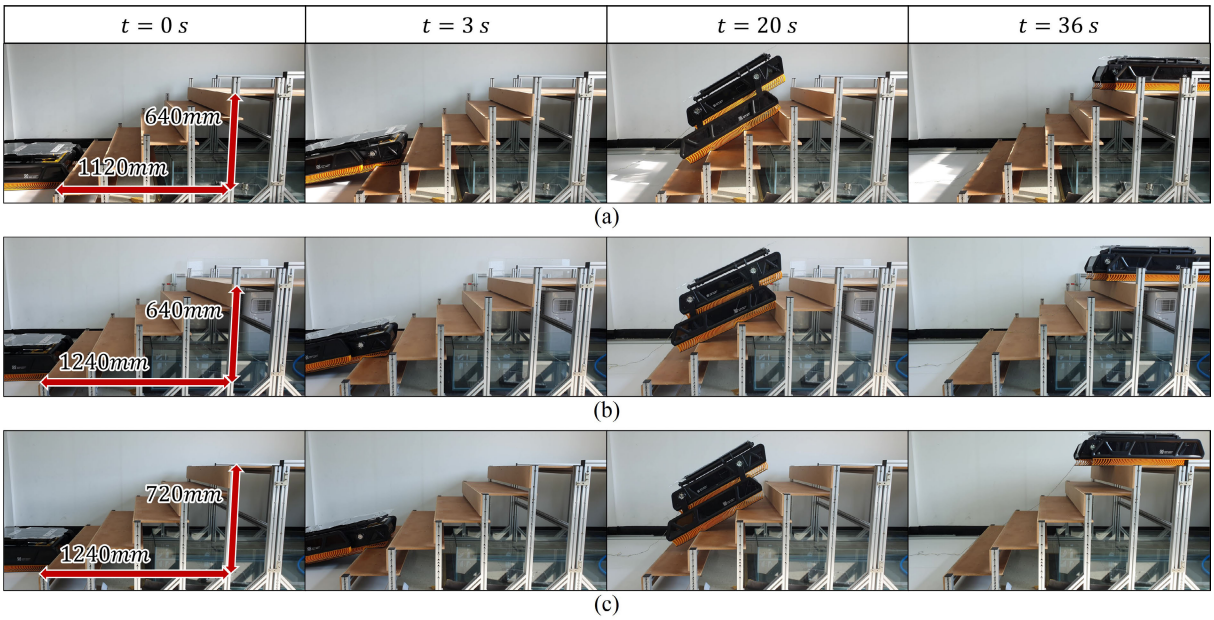

FIGURE 13. Stair-climbing experiment on the test bench. Stair sizes: (a) 280 × 160 mm^2 (b) 310 × 160 mm^2 (c) 310 × 180 mm^2.

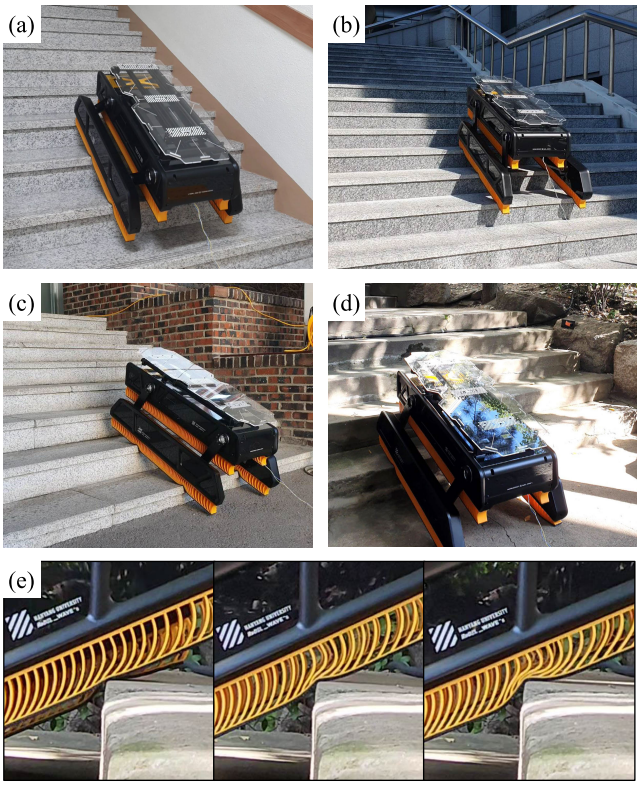

FIGURE 14. Field tests on various stairs. Stair sizes: (a) 288 × 144 mm^2 (b) 299 × 125 mm^2 (c) 359 × 169 mm^2 (d) 365 × 140 mm^2. (e) Gradually deforming soft feet.

step, so they cannot climb stairs smaller than the robot. For tracked robots, the height that the grouser can reach is the height of the stairs that they can climb. So they climb taller stairs by making the track higher [14] or by lifting the track with flippers [12], [13] or assistive brackets [10], [11]. For a tracked robot to climb stairs reliably, the track must touch at least two stairs. Therefore, we define the length R of a stairs that a tracked robot can climb in Table 1 as less than or equal to half the length of the track touching the ground. Tracked robots have simpler controls and faster stair climbing speeds because once they enter the stairs, they can climb the stairs by only rotating their drive wheels. However, tracked robots can have slippage issues depending on the grousers. Legged robots are able to climb most stairs [15], [16], [17]. Their dynamic movements also allow them to climb stairs quickly. However, legged robots require detailed information about the stairs and have more complex mechanisms and controls.

WAVE and WAVES go up a stair for every one turn of the crank. They also require low mechanism complexity and control levels. Fig. 15 shows the range of stairs WAVES and WAVE can theoretically climb and the size of the stairs we tested on the test bench and field. The shape of the grooves determines the size of the stairs WAVE can climb. But the grooves of WAVE are not deformable. Therefore, WAVE can only climb stairs whose diagonal length exceeds 328.67 mm and is less than 350 mm. In contrast, WAVES can climb stairs with $R \leq 400$ mm, which is about half of the robot length. Its because the soft feet change according to the shape of the stairs. To test WAVES' ability to overcome stairs, we conducted experiments on seven different sizes of stairs, six of which WAVE could not climb. Through experiments, we confirmed that soft feet solved the chronic low adaptability problem of the previous study. Each stair-climbing robot has its appropriate field of use due to its strengths and weaknesses. Wheeled robots are fast and efficient when traveling on flat surfaces. Therefore, it is suitable as a delivery robot in environments centered on

flat areas. Track robots can handle rough terrain and move quickly. Additionally, because it can carry heavy weights, it is suitable for wheelchairs that climb stairs or disaster response robots. Legged robots are highly adaptable, but they consume a lot of battery due to their large number of actuators. Therefore, it is suitable for patrol robots traveling on routes that include charging stations. WAVES has a simple structure and can climb stairs reliably and efficiently. Therefore, it is suitable for long-distance delivery that includes many stairs.

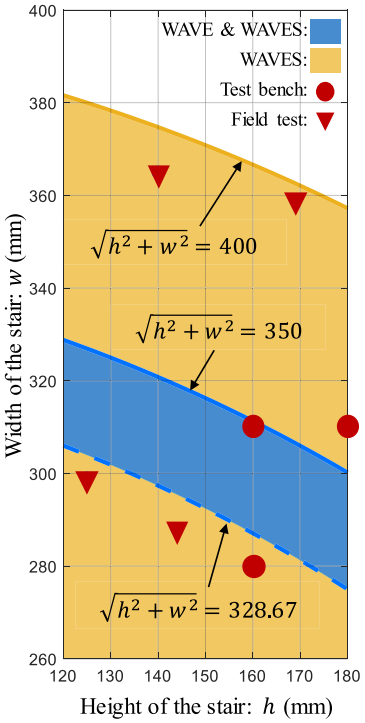

FIGURE 15. Graph showing the range of stairs sizes that WAVE and WAVES can climb. The points represent the size of the stairs that WAVES climbed.

VI. CONCLUSION

This paper proposes WAVES, a stair-climbing robot with adaptability through soft feet. Soft feet can deform according to the environment; therefore, WAVES can climb various types of stairs. We made three types of samples, i.e., arc, honeycomb, and spoke, to determine the patterns of soft feet. Through Ansys simulations, we measured the horizontal and vertical reaction forces that occur when soft feet are pressed against the stairs. The vertical force must be sufficient to withstand the weight of the robot. But the horizontal force pushes the robot away from the stairs, so the smaller is better. We decided to use the ratio of the horizontal and vertical reaction forces of the soft feet pushing the stairs as the index that determines stability. As a result of the simulation, the horizontal force ratio of the arc-shaped pattern was the smallest at 0.224 (honeycomb: 0.303, spoke: 0.276).

We divided the process of climbing stairs into three steps: entering, climbing, and exiting, and presented the role of the soft feet at each step. The soft feet were divided into four areas according to their roles. We calculated the maximum reaction force that each part should withstand for the soft foot to deform properly even on stairs of various sizes. We limited the range of step sizes to a height of 160 mm–180 mm and a width 280 mm–310 mm, such that WAVES demonstrated improved performances in general cases. As a result, each part of the soft feet had different mesh intervals depending on the force to be withstood.

Before we apply the soft feet, the diagonal length of the stairs that WAVES could climb was 328.7 mm–350 mm, but after applying the soft feet, it can climb all stairs under 400 mm. WAVES' ability to overcome stairs is proven through experiment. The experiment was conducted on stairs of seven sizes: $280 \times 160\,\text{mm}^2$, $310 \times 160\,\text{mm}^2$, $310 \times 180\,\text{mm}^2$, $288 \times 144\,\text{mm}^2$, $299 \times 125\,\text{mm}^2$, $359 \times 169\,\text{mm}^2$, and $365 \times 140\,\text{mm}^2$.

WAVES has the advantage of being able to climb various stairs, so it can be used as a delivery robot or wheelchair that climbs stairs. From the perspective of stability, it is considered good performance when soft feet deform to the same depth during stair-climbing. However, the position of the center of gravity changes significantly depending on the rotation angle of the crank; therefore, the magnitude of the force applied to the soft feet changes significantly. Therefore, as the crank rotated, the depth at which the soft feet were compressed continued to vary from 10mm to 30mm. Because the angle of the robot changes depending on the deformation of the soft feet, WAVES has high adaptability but suffers some loss in stability. In future studies, we will determine the length at which the soft feet are constantly compressed. To achieve this, we will shorten the crank length to reduce the changes in the position of the center of gravity. In addition, we will optimize the shape of the soft feet and try a variety of soft materials so that the soft feet can always compressed by a certain amount of displacement. After the optimal soft feet is derived, we will confirm the robustness and reliability of the soft feet through repeated experiments.

REFERENCES

[1] E. Karamipour, S. F. Dehkordi, and M. H. Korayem, "Reconfigurable mobile robot with adjustable width and length: Conceptual design, motion equations and simulation," *J. Intell. Robotic Syst.*, vol. 99, nos. 3–4, pp. 797–814, Sep. 2020.

[2] T. Takaki, T. Aoyama, and I. Ishii, "Development of inverted pendulum robot capable of climbing stairs using planetary wheel mechanism," in *Proc. IEEE Int. Conf. Robot. Autom.*, May 2013, pp. 5618–5624.

[3] (Dec. 2021). *This is Ascento Pro.* [Online]. Available: https://youtu.be/Uxt2wTI0m5o?si=KLl0KXs0_R_2Ou1e

[4] G. Quaglia, W. Franco, and R. Oderio, "Wheelchair. Q, a motorized wheelchair with stair climbing ability," *Mechanism Mach. Theory*, vol. 46, no. 11, pp. 1601–1609, Nov. 2011.

[5] M. M. Dalvand and M. M. Moghadam, "Stair climber smart mobile robot (MSRox)," *Auto. Robots*, vol. 20, no. 1, pp. 3–14, 2006.

[6] M. Shino, N. Tomokuni, G. Murata, and M. Segawa, "Wheeled inverted pendulum type robotic wheelchair with integrated control of seat slider and rotary link between wheels for climbing stairs," in *Proc. IEEE Int. Workshop Adv. Robot. Its Social Impacts*, Sep. 2014, pp. 121–126.

[7] D. Zhang, J. Xuan, Y. Yang, and Z. Guo, "The design of a scissor stair climbing robot," in *Proc. 7th Int. Conf. Autom., Robot. Appl. (ICARA)*, Feb. 2021, pp. 10–15.

[8] C. Liu, X. Zhang, R. Wu, S. Wang, R. Wang, Z. Lu, Y. Xiao, S. Li, and Z. Wu, "Mechanical design and wheel–leg–body cooperation control of a step-climbing robot," *J. Field Robot.*, vol. 39, no. 7, pp. 1054–1068, Oct. 2022.

[9] Y. Ma and F. Lyu, "Design of a wheel-legged stair climbing robot," in *Proc. 7th Int. Conf. Control, Autom. Robot. (ICCAR)*, Apr. 2021, pp. 146–150.
[10] W. Tao, Y. Jia, T. Liu, J. Yi, H. Wang, and Y. Inoue, "A novel wheel-track hybrid electric powered wheelchair for stairs climbing," *J. Adv. Mech. Design, Syst., Manuf.*, vol. 10, no. 4, 2016, Art. no. JAMDSM0060.
[11] (Sep. 2023). *Scewo BRO Guide | How to Drive Single Steps*. [Online]. Available: https://youtu.be/5lgf1gHVDcs?si=iZnJIueqM-g5-slG
[12] P. Dong, X. Wang, H. Xing, Y. Liu, and M. Zhang, "Design and control of a tracked robot for search and rescue in nuclear power plant," in *Proc. Int. Conf. Adv. Robot. Mechatronics (ICARM)*, Aug. 2016, pp. 330–335.
[13] Y. Liu and G. Liu, "Track-stair interaction analysis and online tipover prediction for a self-reconfigurable tracked mobile robot climbing stairs," *IEEE/ASME Trans. Mechatronics*, vol. 14, no. 5, pp. 528–538, Oct. 2009.
[14] K. Yoneda, Y. Ota, and S. Hirose, "High-grip stair climber with powder-filled belts," *Int. J. Robot. Res.*, vol. 28, no. 1, pp. 81–89, Jan. 2009.
[15] D. Lu, E. Dong, C. Liu, M. Xu, and J. Yang, "Design and development of a leg-wheel hybrid robot," in *Proc. IEEE/RSJ Int. Conf. Intell. Robots Syst.*, Oct. 2013, pp. 6031–6036.
[16] M. Hutter, C. Gehring, D. Jud, A. Lauber, C. D. Bellicoso, V. Tsounis, J. Hwangbo, K. Bodie, P. Fankhauser, M. Bloesch, R. Diethelm, S. Bachmann, A. Melzer, and M. Hoepflinger, "ANYmal—A highly mobile and dynamic quadrupedal robot," in *Proc. IEEE/RSJ Int. Conf. Intell. Robots Syst. (IROS)*, Oct. 2016, pp. 38–44.
[17] A. Bouman, M. F. Ginting, N. Alatur, M. Palieri, D. D. Fan, T. Touma, T. Pailevanian, S.-K. Kim, K. Otsu, J. Burdick, and A.-A. Agha-Mohammadi, "Autonomous spot: Long-range autonomous exploration of extreme environments with legged locomotion," in *Proc. IEEE/RSJ Int. Conf. Intell. Robots Syst. (IROS)*, Oct. 2020, pp. 2518–2525.
[18] X. Chen, J. Yao, S. Zhang, K. Zhu, S. Kong, S. Qi, and X. Zhang, "WebGripper: Bioinspired cobweb soft gripper for adaptable and stable grasping," *IEEE Trans. Robot.*, vol. 39, no. 4, pp. 3059–3071, 2023.
[19] J.-Y. Lee, Y.-S. Seo, C. Park, J.-S. Koh, U. Kim, J. Park, H. Rodrigue, B. Kim, and S.-H. Song, "Shape-adaptive universal soft parallel gripper for delicate grasping using a stiffness-variable composite structure," *IEEE Trans. Ind. Electron.*, vol. 68, no. 12, pp. 12441–12451, Dec. 2021.
[20] X. Shan and L. Birglen, "Modeling and analysis of soft robotic fingers using the fin ray effect," *Int. J. Robot. Res.*, vol. 39, no. 14, pp. 1686–1705, Dec. 2020.
[21] Y.-S. Seo, J.-Y. Lee, C. Park, J. Park, B.-K. Han, J.-S. Koh, U. Kim, H. Rodrigue, J. Bak, and S.-H. Song, "Highly shape-adaptable honeycomb gripper using orthotropic surface tension," *IEEE Trans. Ind. Electron.*, vol. 7, no. 3, pp. 2662–2671, 2024.
[22] (Dec. 2018). *NAMU*. [Online]. Available: https://www.youtube.com/watch?v=pyCgcX9fKlc
[23] *Soft-Bodied Robots: Re-Shaping the Future of Mobility | Amoeba Energy*. Accessed: Jan. 22, 2024. [Online]. Available: https://en.amoebaenergy.com/product/
[24] S. Park, S. Ahn, J. Shin, H. Kim, J. Yang, Y. Kim, K. Lim, and T. Seo, "WAVE: Last mile delivery robotic platform with stair-climbing ability via four-bar linkage-based locomotion," *IEEE/ASME Trans. Mechatronics*, pp. 1–11, 2023, doi: 10.1109/TMECH.2023.3275919.
[25] H. Nakano and S. Hirose, "Crank-wheel: A brand new mobile base for field robots," in *Proc. IEEE/RSJ Int. Conf. Intell. Robots Syst.*, Oct. 2012, pp. 4608–4613.
[26] H. Komura, G. Endo, and K. Suzumori, "Eccentric Crank rover: A novel Crank wheel mechanism with eccentric wheels," in *Proc. IEEE/RSJ Int. Conf. Intell. Robots Syst. (IROS)*, Oct. 2016, pp. 1048–1053.
[27] Y. Liu, H. Kim, and T. Seo, "AnyClimb: A new wall-climbing robotic platform for various curvatures," *IEEE/ASME Trans. Mechatronics*, vol. 21, no. 4, pp. 1812–1821, Aug. 2016.
[28] Y. Liu and T. Seo, "Anyclimb-II: Dry-adhesive linkage-type climbing robot for uneven vertical surfaces," *Mech. Mach. Theory*, vol. 124, pp. 197–210, Jun. 2018.
[29] C. Nie, X. Pacheco Corcho, and M. Spenko, "Robots on the move: Versatility and complexity in mobile robot locomotion," *IEEE Robot. Autom. Mag.*, vol. 20, no. 4, pp. 72–82, Dec. 2013.
[30] T. Seo, S. Ryu, J. H. Won, Y. Kim, and H. S. Kim, "Stair-climbing robots: A review on mechanism, sensing, and performance evaluation," *IEEE Access*, vol. 11, pp. 60539–60561, 2023.
[31] J. Phromjan and C. Suvanjumrat, "The modification of steel belt layer of airless tire for finite element analysis," *IOP Conf. Series, Mater. Sci. Eng.*, vol. 773, no. 1, Feb. 2020, Art. no. 012047.
[32] (Jun. 2019). *New Generation of Airless Tire | Michelin*. [Online]. Available: https://www.youtube.com/watch?v=VjiLzc9bD3Q&t=2s
[33] S. Shashavalli, C. R. Reddy, G. K. Yadiki, "Design and analysis of four wheeler airless tire," *Int. J. Adv. Technol. Innov. Res.*, vol. 8, no. 2, pp. 4298–4305, 2016.
[34] M. Ramachandran, "Nonlinear finite element analysis of tweel geometric parameter modifications on spoke dynamics during high speed rolling," Ph.D. dissertation, Dept. Mech. Eng., Clemson Univ., Clemson, SC, USA, 2008.
[35] T. Bitzer, *Honeycomb Technology: Materials, Design, Manufacturing, Applications and Testing*. Berlin, Germany: Springer, 1997.

SUNGJUN PARK received the B.S. degree in mechanical engineering from Hanyang University, in 2022, where he is currently pursuing the M.S. degree in mechanical convergence engineering. His research interest includes robot mechanism design.

JEONGPIL SHIN (Member, IEEE) received the B.S. degree in mechanical engineering from Hanyang University, in 2020, where he is currently pursuing the M.S. degree in mechanical convergence engineering. His research interest includes robot mechanism design.

YOUNGHWAN KIM received the B.S. degree in mechanical engineering from Hanyang University, in 2022, where he is currently pursuing the M.S. degree in mechanical convergence engineering. His research interest includes robot mechanism design.

TAEWON SEO (Senior Member, IEEE) received the B.S. and Ph.D. degrees from the School of Mechanical and Aerospace Engineering, Seoul National University, South Korea, in 2003 and 2008, respectively. He is currently a Professor with the School of Mechanical Engineering and the Director of the Robot Design Engineering Laboratory, Hanyang University, South Korea. Before Hanyang University, he was a Postdoctoral Researcher with the Nanorobotics Laboratory, Carnegie Mellon University; a Visiting Professor with the Biomimetic Millisystems Laboratory, UC Berkeley; a Visiting Scholar with the University of Michigan; and an Associate Professor with the School of Mechanical Engineering, Yeungnam University, South Korea. His research interests include robot design, analysis, control, optimization, and planning. He received the Best Paper Award of IEEE/ASME TRANSACTIONS ON MECHATRONICS, in 2014. He was a Technical/Associate Editor of IEEE/ASME TRANSACTIONS ON MECHATRONICS and IEEE ROBOTICS AND AUTOMATION LETTERS and is an Associate Editor of *Intelligent Service Robots* and *International Journal of Precision Engineering and Manufacturing*.